

Cite this: DOI: 10.1039/c4gc00178h

Highly active, water-compatible and easily separable magnetic mesoporous Lewis acid catalyst for the Mukaiyama–Aldol reaction in water†

Fang Zhang,* Xiaotao Wu, Chao Liang, Xiaoyan Li, Zhen Wang and Hexing Li*

A novel magnetic mesoporous Lewis acid catalyst was prepared through immobilizing $\text{Yb}(\text{OTf})_3$ on a sodium propylsulphonate and phenyl group co-functionalized magnetic core–mesoporous silica shell composite. The obtained $\text{Yb}(\text{OTf})_2\text{-SO}_3\text{Na}\&\text{Ph-MCMSS}$ catalyst had a typical core–shell structure with a Fe_3O_4 magnetic core, a middle amorphous silica layer and a multifunctional mesoporous silica shell with radial pore channels. In water medium Mukaiyama–Aldol reactions, it exhibited a higher catalytic reactivity than that of the homogeneous catalyst $\text{Yb}(\text{OTf})_3$, and control catalysts $\text{Yb}(\text{OTf})_2\text{-SO}_3\text{Na-MCMSS}$ without phenyl groups inside the mesoporous channels, $\text{Yb}(\text{OTf})_2\text{-SO}_3\text{Na}\&\text{Ph-MCSS}$ without a mesoporous structure, mesoporous $\text{Yb}(\text{OTf})_2\text{-SO}_3\text{Na}\&\text{Ph-MCM-41}$ with an irregular morphology and nonporous $\text{Yb}(\text{OTf})_2\text{-SO}_3\text{Na-Amberlyst-15}$ ion-exchange resin. The systematic analysis demonstrated that this excellent catalytic performance could be attributed to the synergetic effect resulting from its radial mesoporous channels and the pore surface hydrophobicity, leading to the increased accessibility of active sites and the decreased diffusion limitation of reactants. More importantly, this catalyst was stable in water and could be easily separated with a simple magnet and reused at least six times without loss of catalytic activity.

Received 3rd February 2014,
Accepted 21st March 2014

DOI: 10.1039/c4gc00178h

www.rsc.org/greenchem

1. Introduction

Homogeneous acid catalysts are mostly common used in the large-scale production of industrial chemicals and fine chemicals.¹ However, their inherent drawbacks such as the corrosivity, the environmental hazards as well as the high cost of separating the acids from the reaction system, make it very difficult to meet the requirements of environmentally friendly chemical processes.² Moreover, some of them generally must be used under anhydrous conditions, which necessitates massive toxic, flammable organic solvents and specialized reaction vessels.³ On the contrary, enzymes have an unparalleled ability to accomplish many biological processes in aqueous medium, which has inspired significant research activities in the development of solid acid catalysts for chemical synthesis in water.⁴ The remarkable advantages of this catalytic system are that it could simultaneously reduce the pollution and cost resulting from liquid acids and organic solvents, coupled with the ease of recovery and recycling of homo-

geneous acid catalysts. Although extensive efforts have been devoted to the fabrication of solid acid catalysts, they usually display inferior catalytic efficiencies in water-medium organic syntheses compared to their homogeneous counterparts. The intrinsic problems in the heterogeneous catalytic systems are the decreased accessibility of active sites and the enhanced diffusion limitation of reactants, leading to the declined catalytic reactivity and selectivity.⁵ Recently, homogeneous acids immobilized on a solid matrix with a high surface area or nanoscale size represented a viable solution to this problem because these supports could guarantee the high dispersion of active sites and reduce the mass transfer resistance.⁶ However, the consequent challenge is that conventional separation methods such as filtration or centrifugation may become inefficient for these nanocatalysts.⁷ To overcome this drawback, magnetically supported acid catalysts have received increasing attention since they can be easily removed from the reaction mixture by external magnetic separation.⁸ Nevertheless, the low surface area and rapid aggregation of the typical iron oxide support make it difficult to maximize catalyst dispersion and activity.⁹ Meanwhile, the rare functionality of the iron oxide surface limits the optimization of the surface chemistry, such as the hydrophobicity property, resulting in unfavorable chemical microenvironments for water-medium organic reactions.¹⁰ Therefore, one strategy for the fabrication

The Education Ministry Key Lab of Resource Chemistry and Shanghai Key Laboratory of Rare Earth Functional Materials, Shanghai Normal University, Shanghai 200234, P. R. China. E-mail: zhangfang@shnu.edu.cn, HeXing-Li@shnu.edu.cn

† Electronic supplementary information (ESI) available. See DOI: 10.1039/c4gc00178h

of highly active, water-compatible and easily separable solid acid catalysts for chemical synthesis in water, is to form multi-functional nanocomposites that combine the advantages of both a nanoporous support and magnetic material, which favor a high surface area, tunable chemical composition and convenient separation.

Magnetic mesoporous materials have attracted enormous interest for the development of novel heterogeneous catalysts owing to their outstanding features, such as unique magnetic response, large surface area, tunable pore structure and surface functionality.¹¹ In this context, magnetic core-mesoporous silica shell (MCMSS) composites that are comprised of a superparamagnetic Fe_3O_4 core and an outer shell of ordered mesoporous silica with radial pore channels have great potential. Owing to their distinctive advantages of both short pore channels and highly open pore structure, several different MCMSS supported catalysts containing metal nanoparticles or metal oxides have shown remarkable enhancements of catalytic activity.¹² However, to the best of our knowledge, Lewis acids bonded to the mesoporous channel of a MCMSS support for water-medium organic synthesis has not been reported so far. Additionally, insight into the adsorption and diffusion behaviors in the confined microenvironment of the MCMSS supported catalysts has been rarely discussed. Herein, we report for the first synthesis of a novel magnetic mesoporous Lewis acid catalyst ($\text{Yb}(\text{OTf})_2\text{-SO}_3\text{Na\&Ph-MCMSS}$) through immobilizing $\text{Yb}(\text{OTf})_3$ on a sodium propylsulphonate and phenyl group co-functionalized magnetic core-mesoporous silica shell composite. It should be noted that the catalyst exhibited a higher activity compared to the homogeneous catalyst $\text{Yb}(\text{OTf})_3$ and control catalysts (including $\text{Yb}(\text{OTf})_2\text{-SO}_3\text{Na-MCMSS}$ without phenyl groups inside the mesoporous channels, $\text{Yb}(\text{OTf})_2\text{-SO}_3\text{Na\&Ph-MCSS}$ without a mesoporous structure, $\text{Yb}(\text{OTf})_2\text{-SO}_3\text{Na\&Ph-MCSS}$ mesoporous catalyst with an irregular morphology and a nonporous $\text{Yb}(\text{OTf})_2\text{-SO}_3\text{Na-Amberlyst-15}$ ion-exchange resin), in the water-medium Mukaiyama–Aldol reaction. This excellent catalytic performance could be attributed to the synergic effect resulting from the radially short mesoporous channels and the surface hydrophobicity, which efficiently enriched the reactants and meanwhile decreased the mass transfer limitation. Moreover, it could be easily separated using an external magnet and reused up to 6 times without loss of catalytic activity.

2. Experimental section

2.1. Sample preparation

2.1.1. Synthesis of amorphous silica coated Fe_3O_4 microspheres ($\text{SiO}_2@\text{Fe}_3\text{O}_4$). Fe_3O_4 microspheres were prepared according to the method previously described by Zhao *et al.*^{12a} In a typical run, 0.12 g Fe_3O_4 was added to 100 ml HCl aqueous solution (0.10 M) and then the mixture was treated by ultrasonication for 30 min and washed by ethanol and water. The solid was filtrated and subsequently dispersed in a solution containing 160 ml ethanol and 30 ml deionized water.

The solution was adjusted to pH 10 by 28 wt% aqueous ammonia solution. After that, 0.25 ml tetraethyl orthosilicate (TEOS) was introduced into the solution at 25 °C under mechanical stirring for 6 h. The products were collected and washed with ethanol and water, followed by drying at 60 °C for 12 h.

2.1.2. Preparation of the multifunctional magnetic mesoporous silica support ($\text{SO}_3\text{Na\&Ph-MCMSS}$). 0.20 g $\text{SiO}_2@\text{Fe}_3\text{O}_4$ particles were dispersed in an aqueous solution containing 0.64 g CTAB, 100 ml deionized water, 2.0 ml ammonia solution (28 wt%), and 140 ml ethanol. This mixture was ultrasonicated for 30 min and then mechanically stirred for another 30 min. Then, 0.625 ml TEOS was added dropwise to the above solution. After pre-hydrolysis for 30 min, 0.116 ml mercaptopropyltrimethoxysilane (MPTS) and 0.117 ml phenyltrimethoxysilane (PhTS) were introduced. After stirring for 12 h at 25 °C, the products were collected with a magnet and washed repeatedly with ethanol and deionized water. Finally, the CTAB template was removed by repeated ethanol extraction under reflux conditions. Next, 0.20 g of the solid sample was suspended in 30 ml H_2O_2 solution and stirred for 24 h. The obtained solid was washed and then added to 30 ml saturated NaCl solution for ion-exchange treatment, resulting in a sodium propylsulphonate and phenyl group co-functionalized magnetic core-mesoporous silica shell composite.

2.1.3. Fabrication of the magnetic mesoporous Lewis acid catalyst ($\text{Yb}(\text{OTf})_2\text{-SO}_3\text{Na\&Ph-MCMSS}$). The $\text{SO}_3\text{Na\&Ph-MCMSS}$ support was introduced into a 35 ml ethanol solution containing 0.50 g $\text{Yb}(\text{OTf})_3$ under mechanical stirring for 3 h at 80 °C. The black powder product was filtered and washed thoroughly with absolute ethanol to eliminate any un-coordinated $\text{Yb}(\text{OTf})_3$ compound, followed by vacuum drying at 60 °C for 24 h.

2.2. Characterization

The ytterbium loading was measured by an inductively coupled plasma optical emission spectrometer (Varian VISTA-MPX). The sulfur content was determined by elemental analysis on an Element Vario EL III analyzer. Fourier transform infrared (FTIR) spectra were obtained using a Thermo Nicolet Magna 550 spectrometer. The X-ray powder diffraction (XRD) data was acquired on a Rigaku D/maxr B diffractometer using $\text{Cu K}\alpha$ radiation. N_2 adsorption-desorption isotherms were analyzed by a Quantachrome NOVA 4000e analyzer. Specific surface areas (S_{BET}) and average pore diameters (D_p) are calculated using BET and BJH models, respectively. The morphologies were observed by transmission electron microscopy (TEM, JEM-2011). The surface electronic states were analyzed by X-ray photoelectron spectroscopy (XPS, Perkin-Elmer PHI 5000C ESCA). All the binding energy values were calibrated by using $\text{C}_{1s} = 284.6$ eV as a reference. The magnetic property was measured by a superconducting quantum interference device magnetometer (SQUID). The hysteresis loops of these samples were recorded at temperatures of 300 K. Water and toluene vapour absorption measurements were carried out on an intelligent gravimetric analyser (Hidden Isochema IGA-002/3) by introducing a dosed amount of high-

purity vapor directly into the sample chamber and recording the weight change after a stable equilibrium pressure was reached.

2.3. Activity test

In a typical run of the water-medium Mukaiyama–Aldol reaction, a catalyst containing 0.050 mmol Yb(III), 0.5 mmol benzaldehyde, 1.0 mmol trimethyl-(1-phenylprop-1-enyloxy)silane and 3.0 ml distilled water were mixed and allowed to react at 20 °C for 16 h under mild stirring. The products were extracted with ethyl acetate, followed by analysis on a high performance liquid chromatography analyzer (HPLC, Agilent 6410 series Triple Quad) equipped with an Agilent C18 column. The reaction conversion was calculated based on benzaldehyde since trimethyl(1-phenylprop-1-enyloxy)silane was in excess.

In order to determine the catalyst recyclability, the catalyst was allowed to settle down by a magnet after each run of reaction and the clear supernatant liquid was decanted slowly. The residual solid catalyst was reused with a fresh charge of water and reactant for subsequent cycles under the same reaction conditions. In all the tests, the reproducibility was checked by repeating each result at least three times and was found to be within $\pm 5\%$. Meanwhile, the liquid phase of the reaction mixture was collected for ICP analysis after each reaction to test for Yb leaching.

2.4. Adsorption test

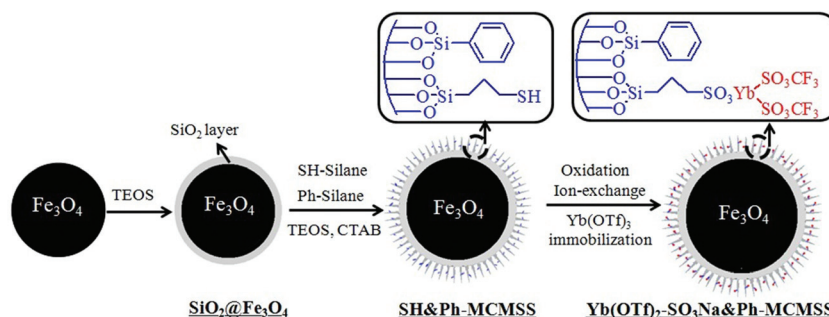
To determine the adsorption performances of the magnetic catalysts, 50 mg catalyst was firstly soaked in 100 ml water and oscillated at 25 °C for 12 h. Then, 100 ml aqueous solution including 10 ppm benzaldehyde was added into the above solution. The solution was sampled at given time intervals and the concentration of the remaining benzaldehyde in the solution was determined on a HPLC analyzer. The adsorption capacity was measured after reaching the saturation adsorption.

3. Results and discussion

The synthetic protocol used to achieve the magnetic mesoporous Yb(OTf)₂-SO₃Na&Ph-MCMSS catalyst is presented in

Scheme 1. We started by depositing a thin silica layer on the prefabricated Fe₃O₄ microspheres through a sol-gel coating strategy and then employed a surfactant-directed assembly approach to further generate the thiol- and phenyl-functionalized mesostructured silica/CTAB composite on the SiO₂@Fe₃O₄ surface by using cetyltrimethyl ammonium bromide (CTAB) as a pore template, tetraethyl orthosilicate [TEOS, Si(OEt)₄], mercaptopropyltrimethoxysilane [MPTS, SH-(CH₂)₃Si(OMe)₃] and phenyltrimethoxysilane [PTS, PhSi(OMe)₃] as functional precursors. After removing CTAB by ethanol extraction, this bifunctionalized magnetic core-mesoporous silica shell composite was treated by H₂O₂ oxidation and the subsequent NaCl ion-exchange processes, resulting in the SO₃Na and Ph groups co-functionalized support (SO₃Na&Ph-MCMSS). Then, the Yb(III) Lewis acids can be introduced into the mesoporous channels of the SO₃Na&Ph-MCMSS support by exposure to the Yb(OTf)₃ solution to form the final catalyst, denoted as Yb(OTf)₂-SO₃Na&Ph-MCMSS. For comparison, Yb(III) Lewis acids immobilized on the SO₃Na-functionalized magnetic core-mesoporous silica shell support without hydrophobic phenyl groups inside the mesoporous channels, named as Yb(OTf)₂-SO₃Na-MCMSS, was also synthesized using a similar protocol. Also, Yb(III) Lewis acids grafted on the SO₃Na- and Ph-functionalized magnetic core-silica shell support without a mesoporous structure, denoted as Yb(OTf)₂-SO₃Na&Ph-MCSS, were prepared through directly coordinating Yb(OTf)₃ with SO₃Na and Ph groups terminally bonded to the SiO₂@Fe₃O₄ microspheres (Scheme S1†). Meanwhile, two non-magnetic control catalysts were fabricated including Yb(OTf)₂-SO₃Na&Ph-MCM-41, which was prepared by immobilizing Yb(OTf)₃ in the SO₃Na- and Ph-functionalized traditional mesoporous support MCM-41, and the Yb(OTf)₂-SO₃Na-Amberlyst-15 catalyst was synthesized by immobilizing Yb(OTf)₃ on the SO₃Na-functionalized commercial ion-exchange resin Amberlyst-15.

We firstly optimized the sulfur content of the functionalized support through variation of the molar ratio between TEOS and MPTS silanes and obtained a 1.39 mmol g⁻¹ sulfur content in the SO₃Na&Ph-MCMSS support (Table S1†). Next, we investigated the immobilization conditions using different solvents and the molar ratio between the Yb(OTf)₃ catalyst and the SO₃Na-ligands, resulting in an optimal catalyst with



Scheme 1 Schematic illustration of the synthesis of the magnetic mesoporous Yb(OTf)₂-SO₃Na&Ph-MCMSS catalyst.

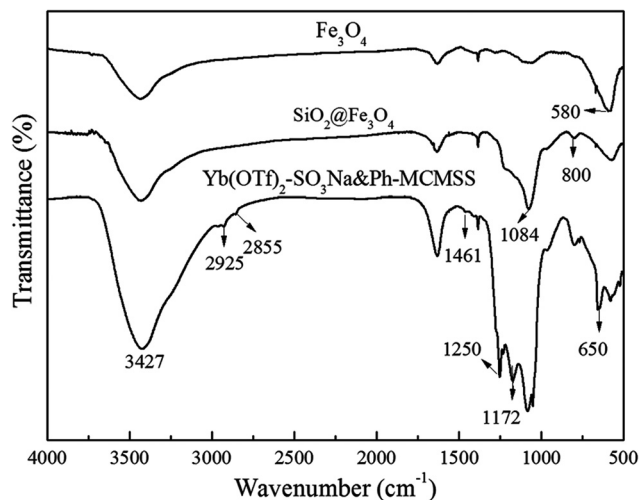


Fig. 1 FTIR spectra of the Fe_3O_4 , $\text{SiO}_2@\text{Fe}_3\text{O}_4$ and $\text{Yb}(\text{OTf})_2\text{-SO}_3\text{Na}\&\text{Ph-MCMSS}$ samples.

0.265 mmol g^{-1} $\text{Yb}(\text{III})$ loading (Table S2†). The $\text{Yb}(\text{OTf})_2\text{-SO}_3\text{Na}\&\text{Ph-MCMSS}$ catalyst was characterized before and after each functionalization step. The FT-IR spectra (Fig. 1) revealed that the as-made Fe_3O_4 microspheres displayed a vibration band at 580 cm^{-1} , which is indicative of the typical Fe–O bond.¹³ The $\text{SiO}_2@\text{Fe}_3\text{O}_4$ sample showed new broad peaks at 1084 and 800 cm^{-1} , which were attributed to the asymmetric stretching bonds of Si–O–Si,¹⁴ suggesting the successful coating of a thin silica layer on the Fe_3O_4 surface. In comparison with the $\text{SiO}_2@\text{Fe}_3\text{O}_4$ sample, the $\text{Yb}(\text{OTf})_2\text{-SO}_3\text{Na}\&\text{Ph-MCMSS}$ sample exhibited several additional absorption peaks. Two additional absorbance peaks around 650 and 1461 cm^{-1} were indicative of the $\delta_{\text{C-H}}$ and $\nu_{\text{C-C}}$ vibrations of the phenyl groups while two additional absorbance bands around 2925 and 2855 cm^{-1} were attributed to the asymmetric and symmetric stretching modes of the C–H bond in the propyl groups, revealing the co-existence of phenyl and SO_3Na moieties.¹⁵ Meanwhile, the new peak around 1172 cm^{-1} was

ascribed to the C–F stretching absorption of the CF_3 groups. In addition, the sulfate stretching vibration absorption at 1250 cm^{-1} could also be found.¹⁶ These results clearly demonstrated the successful incorporation of the $\text{Yb}(\text{OTf})_3$ complex in the multifunctional magnetic mesoporous silica support.

The chemical state of the $\text{Yb}(\text{OTf})_2\text{-SO}_3\text{Na}\&\text{Ph-MCMSS}$ catalyst was investigated by its XPS spectrum. As shown in Fig. 2, the results revealed that the $4\text{d}_{5/2}$ and $4\text{d}_{3/2}$ electronic states of all the Yb species in the $\text{Yb}(\text{OTf})_2\text{-SO}_3\text{Na}\&\text{Ph-MCMSS}$ catalyst were observed at 187.6 eV and 202.6 eV , suggesting that the Yb element was present in a trivalent oxidation state.¹⁷ In comparison with the $\text{Yb}(\text{OTf})_3$ sample, the binding energy of the ytterbium species in the $\text{Yb}(\text{OTf})_2\text{-SO}_3\text{Na}\&\text{Ph-MCMSS}$ catalyst was shifted negatively by 0.70 eV . This shift could be ascribed to the stronger electron-donating property of the sulfur element in the propylsulphonate groups than that in the triflate ligands. This explanation could be further confirmed by XPS analysis of the sulfur element. The binding energy of the sulfur species in the $\text{Yb}(\text{OTf})_2\text{-SO}_3\text{Na}\&\text{Ph-MCMSS}$ catalyst shifted positively by 0.40 eV compared to the $\text{Yb}(\text{OTf})_3$ sample. Thus, the presence of the electron transfer between $\text{Yb}(\text{OTf})_3$ and functionalized support correlated with the observation of the FT-IR spectrum, confirming that the $\text{Yb}(\text{III})$ Lewis acid was immobilized by replacing one triflate ligand in $\text{Yb}(\text{OTf})_3$ with a SO_3Na ligand in the mesoporous channels of the $\text{SO}_3\text{Na}\&\text{Ph-MCMSS}$ support.

We then investigated the morphological properties of the $\text{Yb}(\text{OTf})_2\text{-SO}_3\text{Na}\&\text{Ph-MCMSS}$ catalyst. The TEM image (Fig. 3a) indicated that it had a regular spherical shape with around 500 nm size. It further revealed that a typical core-shell structure of the $\text{Yb}(\text{OTf})_2\text{-SO}_3\text{Na}\&\text{Ph-MCMSS}$ catalyst was formed with the magnetic core (Fe_3O_4 , dark) surrounded by a silica shell (SiO_2 , bright). Moreover, the silica shell consisted of a middle thin silica shell with a thickness of *ca.* 15 nm and a top mesoporous silica shell with a thickness of about 70 nm . Notably, the HRTEM image of the $\text{Yb}(\text{OTf})_2\text{-SO}_3\text{Na}\&\text{Ph-MCMSS}$ catalyst (Fig. 3b) demonstrated that wormhole-like mesopores with diameters of *ca.* $2\text{--}3\text{ nm}$ were observed and the pore

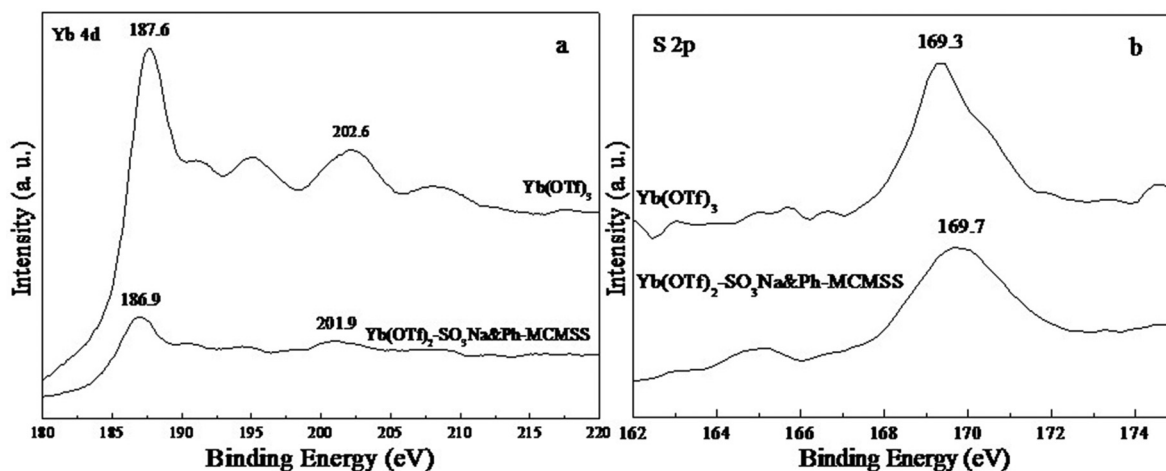


Fig. 2 XPS spectra of the $\text{Yb}(\text{OTf})_2\text{-SO}_3\text{Na}\&\text{Ph-MCMSS}$ catalyst ((a) Yb 4d; (b) S 2p).

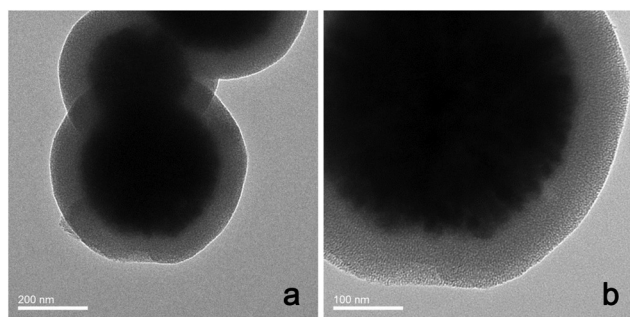


Fig. 3 TEM pictures of the $\text{Yb}(\text{OTf})_2\text{-SO}_3\text{Na}\&\text{Ph-MCMSS}$ catalyst.

channels were radially aligned in the top mesoporous silica shell, which result from the unique co-assembly of CTAB/silica on the surface of the $\text{SiO}_2\text{@Fe}_3\text{O}_4$ microsphere.¹² The meso-structure of the $\text{Yb}(\text{OTf})_2\text{-SO}_3\text{Na}\&\text{Ph-MCMSS}$ catalyst was further analyzed using low-angle XRD analysis. It exhibited a well-resolved diffraction peak at around 2.2° , indicative of the (100) reflection and two other peaks at 3.8° and 4.4° , corresponding to (110) and (200) reflections, suggesting that the hexagonal arrayed pore structure ($p6mm$) could be well preserved after anchoring the Yb Lewis acid catalyst (Fig. 4a).¹⁸ The N_2 sorption curve of the $\text{Yb}(\text{OTf})_2\text{-SO}_3\text{Na}\&\text{Ph-MCMSS}$ sample (Fig. 4b) exhibited a type IV isotherm with the capillary condensation step in the low pressure region and an almost constant adsorption in the high pressure region, confirming the existence of a uniform mesoporous structure.¹⁹ The narrow and sharp pore size distribution profile derived from the adsorption branch (inset) further suggested that the mesopores were uniform. In addition, the calculated BET surface area and total pore volume were $248 \text{ m}^2 \text{ g}^{-1}$ and $0.14 \text{ cm}^3 \text{ g}^{-1}$, indicating a high degree of porosity. Compared to the $\text{SO}_3\text{Na}\&\text{Ph-MCMSS}$ support (Table 1), the $\text{Yb}(\text{OTf})_2\text{-SO}_3\text{Na}\&\text{Ph-MCMSS}$ sample displayed slightly decreased values of S_{BET} , V_{P} and D_{P} due to the presence of the bulky Lewis acid moieties inside the mesoporous channels.

The Mukaiyama–Aldol reaction is an important carbon–carbon bond formation process that has the ability to obtain β -hydroxycarbonyl compounds in a regio-, stereo-, and enantio-selective manner.²⁰ To investigate the utility of our novel $\text{Yb}(\text{OTf})_2\text{-SO}_3\text{Na}\&\text{Ph-MCMSS}$ catalyst, the water-medium Mukaiyama–Aldol reaction of benzaldehyde and trimethyl-(1-phenylprop-1-enyloxy)silane was firstly carried out under the procedure described in the Experimental section. Firstly, the control experiments indicated that the blank experiments with $\text{SiO}_2\text{@Fe}_3\text{O}_4$ and $\text{SH}\&\text{Ph-MCMSS}$ samples could not give any products in the water-medium Mukaiyama–Aldol reaction, indicating that the Yb^{3+} Lewis acid was the active species (Table S3†). Furthermore, the preliminary experiments demonstrated that the optimum reaction temperature was 20°C (Fig. S1†). By adjusting the catalyst amount in the reaction system, the total $\text{Yb}(\text{III})$ amount in each reaction was fixed with a 0.05 mmol loading (Fig. S2†). Under this optimal reaction condition, the $\text{Yb}(\text{OTf})_2\text{-SO}_3\text{Na}\&\text{Ph-MCMSS}$ catalyzed reaction proceeded rapidly and cleanly to the coupling product with 97.2% yield after 16 h (Fig. 5). Interestingly, the homogeneous $\text{Yb}(\text{OTf})_3$ catalyst displayed a significantly decreased catalytic efficiency, with only a 72.4% yield under the same conditions. The different catalytic reactivities of the $\text{Yb}(\text{OTf})_2\text{-SO}_3\text{Na}\&\text{Ph-MCMSS}$ and $\text{Yb}(\text{OTf})_3$ catalysts could be interpreted based on the reaction mechanism. The carbonyl groups in benzaldehyde firstly interact with the $\text{Yb}(\text{III})$ Lewis acid through σ bonding coordination and trimethyl(1-phenylprop-1-enyloxy)silane attacks the activated benzaldehyde to generate the final aldol product. Owing to the low solubility of the two reactants in water, the diffusion and adsorption of the reactants plays a critical role in determining the yield. Therefore, the excellent catalytic reactivity of the $\text{Yb}(\text{OTf})_2\text{-SO}_3\text{Na}\&\text{Ph-MCMSS}$ catalyst could be attributed to the strong surface hydrophobicity derived from the location of the phenyl groups in the mesoporous channels. Accordingly, we used the control $\text{Yb}(\text{OTf})_2\text{-SO}_3\text{Na-MCMSS}$ catalyst without phenyl groups inside the mesoporous channels to confirm the merit of the hydrophobic surface.²¹ As expected, it exhibited a remarkably declined cata-

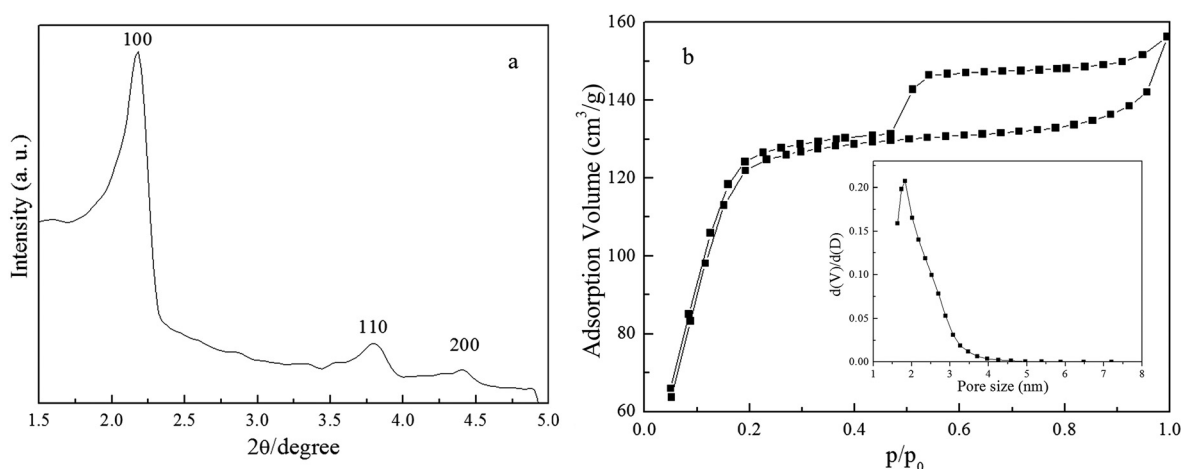
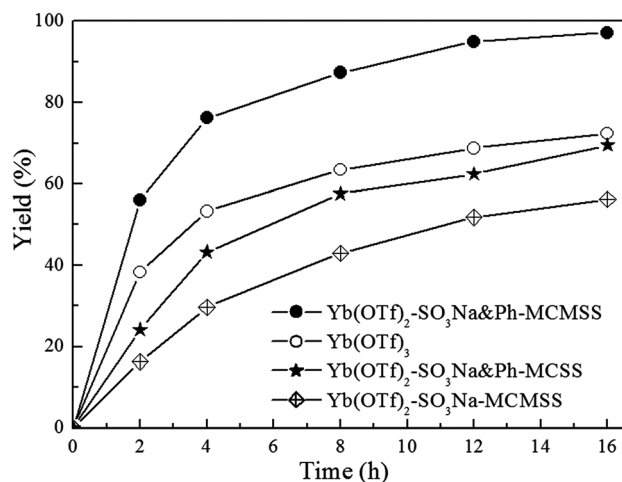
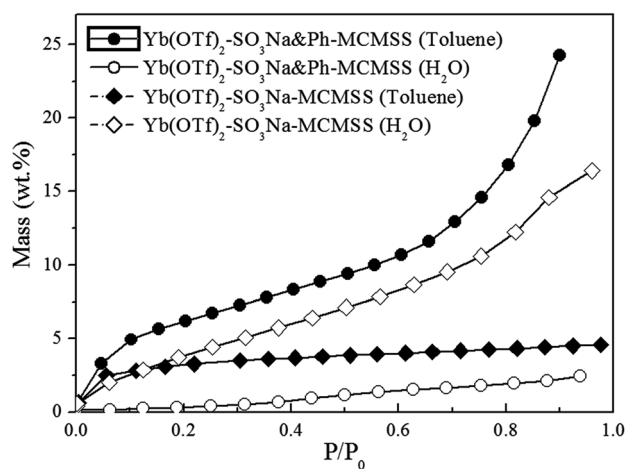


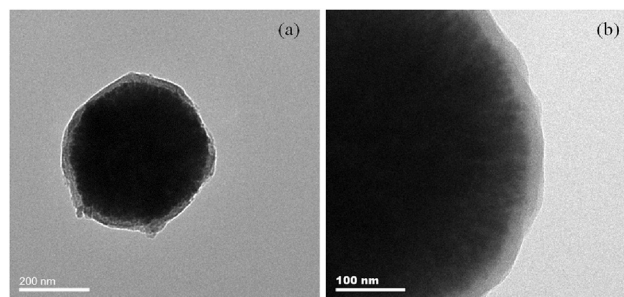
Fig. 4 Low-angle XRD pattern (a), N_2 sorption curve (b) and pore size distribution (inset) of the $\text{Yb}(\text{OTf})_2\text{-SO}_3\text{Na}\&\text{Ph-MCMSS}$ catalyst.

Table 1 Chemical composition and physical parameters of the different Yb catalysts

Sample	S content (mmol g ⁻¹)	Yb loading (mmol g ⁻¹)	S _{BET} (m ² g ⁻¹)	V _p (cm ³ g ⁻¹)	D _p (nm)
SO ₃ Na&Ph-MCMSS	1.39	—	289	0.21	2.5
Yb(OTf) ₂ -SO ₃ Na&Ph-MCMSS	1.39	0.265	248	0.14	2.2
Yb(OTf) ₂ -SO ₃ Na-MCMSS	1.41	0.270	265	0.17	2.3
Yb(OTf) ₂ -SO ₃ Na&Ph-MCSS	0.20	0.0370	36	0.02	1.2
Yb(OTf) ₂ -SO ₃ Na&Ph-MCM-41	1.80	0.385	515	0.55	2.5
Yb(OTf) ₂ -SO ₃ Na-Amberlyst-15	0.17	0.0320	40	—	—

**Fig. 5** Reaction profiles over time in the water-medium Mukaiyama-Aldol reaction between benzaldehyde and trimethyl(1-phenylprop-1-en-1-yl)silane over different catalysts. Reaction conditions are given in Table 1.**Fig. 6** Hydrophobicity tests of the Yb(OTf)₂-SO₃Na&Ph-MCMSS and Yb(OTf)₂-SO₃Na-MCMSS catalysts.

lytic activity with only 56.2% yield. To further validate the enhanced hydrophobicity of the Yb(OTf)₂-SO₃Na&Ph-MCMSS catalyst, both water and toluene absorption experiments were performed (Fig. 6). All the isotherms were of type V, indicative of the weak absorbent-absorbate interactions.²² However, the Yb(OTf)₂-SO₃Na&Ph-MCMSS sample had a higher affinity for

**Fig. 7** TEM images of the Yb(OTf)₂-SO₃Na&Ph-MCSS catalyst.

toluene than that of the Yb(OTf)₂-SO₃Na-MCMSS sample, indicating that it was more hydrophobic. Meanwhile, the adsorption capacity of Yb(OTf)₂-SO₃Na&Ph-MCMSS for toluene (24.2 wt%) was much higher than that of water (2.41 wt%). On the contrary, Yb(OTf)₂-SO₃Na-MCMSS showed the higher adsorption capacity (16.4 wt%) of water than that of toluene (4.59 wt%) and water. These results demonstrated that Yb(OTf)₂-SO₃Na-MCMSS has a selective adsorption for hydrophobic organic substances.

Moreover, the Yb(OTf)₂-SO₃Na&Ph-MCMSS catalyst was more active than the other control Yb(OTf)₂-SO₃Na&Ph-MCSS catalyst with 69.5% yield under the same reaction conditions. Firstly, it had a similar chemical microenvironment with that of the Yb(OTf)₂-SO₃Na&Ph-MCMSS catalyst due to the same Yb(OTf)₃ immobilization approach (Experimental section in ESI†). Moreover, we also calculated the density of Yb(III) active sites in the supports for these two catalysts; the C_{Yb}/S_{BET} value calculated from the Yb content and the specific surface area of the Yb(OTf)₂-SO₃Na&Ph-MCSS and Yb(OTf)₂-SO₃Na&Ph-MCSS catalysts was 1.07×10^{-3} and 1.02×10^{-3} mmol m⁻², respectively. The approximate data confirmed an almost identical active site density. Furthermore, we considered the diffusion distance of the reactants since longer reaction distances decrease the molecular interactions and thus leads to lower catalytic activities.²³ However, the TEM image (Fig. 7) revealed that the Yb(OTf)₂-SO₃Na&Ph-MCSS catalyst was present in uniform spheres with diameters of about 440 nm. Meanwhile, it displayed the core-shell structure with a magnetic core and a thin silica shell of around 30 nm in thickness, demonstrating that the reaction should occur in the catalyst surface without significant diffusion resistance. Therefore, the higher catalytic efficiency of the Yb(OTf)₂-SO₃Na&Ph-MCSS catalyst could be mainly attributed to the existence of a mesoporous structure

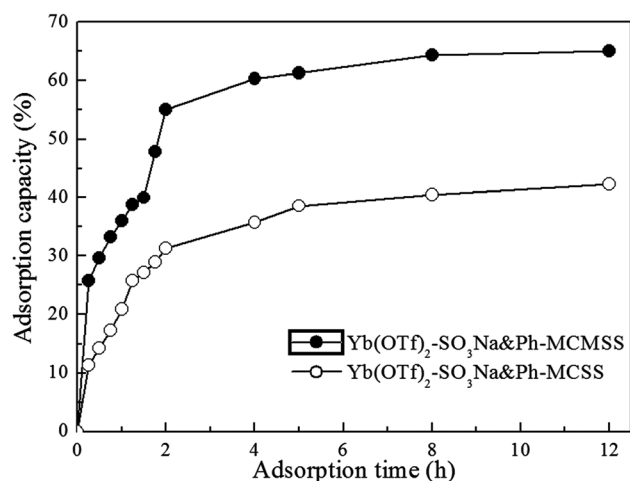


Fig. 8 Benzaldehyde adsorption profiles over the $\text{Yb}(\text{OTf})_2\text{-SO}_3\text{Na&Ph-MCMSS}$ and $\text{Yb}(\text{OTf})_2\text{-SO}_3\text{Na&Ph-MCSS}$ catalysts.

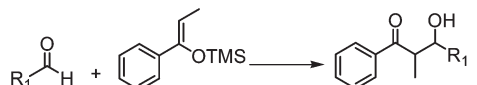
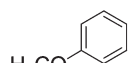
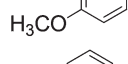
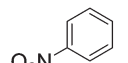
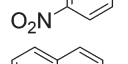
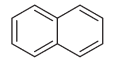
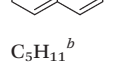
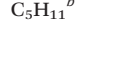
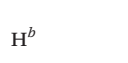

with radial pore alignment, in which the unique confined environments concentrated the reactants and thus led to the enhanced activity.²⁴ In order to prove the above hypothesis, benzaldehyde adsorption tests in water over $\text{Yb}(\text{OTf})_2\text{-SO}_3\text{Na&Ph-MCMSS}$ and $\text{Yb}(\text{OTf})_2\text{-SO}_3\text{Na&Ph-MCSS}$ catalysts were performed. As shown in Fig. 8a, the $\text{Yb}(\text{OTf})_2\text{-SO}_3\text{Na&Ph-MCMSS}$ catalyst displayed a higher saturated adsorption capacity (65.0%) than the $\text{Yb}(\text{OTf})_2\text{-SO}_3\text{Na&Ph-MCSS}$ catalyst (42.3%). Thus, we concluded that the higher enrichment capacity of the organic reactants promoted the catalytic reactivity of the $\text{Yb}(\text{OTf})_2\text{-SO}_3\text{Na&Ph-MCMSS}$ catalyst in water-medium organic reactions.

In addition, we also compared the catalytic performance of the $\text{Yb}(\text{OTf})_2\text{-SO}_3\text{Na-MCMSS}$ catalyst with two non-magnetic

catalysts, including a $\text{SO}_3\text{Na-}$ and Ph- functionalized MCM-41 supported $\text{Yb}(\text{OTf})_3$ catalyst ($\text{Yb}(\text{OTf})_2\text{-SO}_3\text{Na&Ph-MCM-41}$) and a conventional ion-exchange resin supported $\text{Yb}(\text{OTf})_3$ catalyst ($\text{Yb}(\text{OTf})_2\text{-SO}_3\text{Na-Amberlyst-15}$). The XRD pattern, N_2 sorption isotherm and TEM image of $\text{Yb}(\text{OTf})_2\text{-SO}_3\text{Na&Ph-MCM-41}$ demonstrated its two-dimensional hexagonal ordered mesoporous structure. However, the SEM images revealed that it displayed an irregular morphology with a very broad particle size distribution (Fig. S3†). The SEM and TEM images of the $\text{Yb}(\text{OTf})_2\text{-SO}_3\text{Na-Amberlyst-15}$ catalyst showed that it was a nonporous solid (Fig. S4†). Under the same reaction conditions (Table S3†), $\text{Yb}(\text{OTf})_2\text{-SO}_3\text{Na&Ph-MCM-41}$ obtained a relatively high yield of 87.3%, while $\text{Yb}(\text{OTf})_2\text{-SO}_3\text{Na-Amberlyst-15}$ achieved a yield of 75.4%. The inferior catalytic efficiency of $\text{Yb}(\text{OTf})_2\text{-SO}_3\text{Na&Ph-MCM-41}$ could be attributed to its increased diffusion resistance, while the low surface area of $\text{Yb}(\text{OTf})_2\text{-SO}_3\text{Na-Amberlyst-15}$ caused the decreased catalytic activity (Table 1), furthermore demonstrating the advantage of the $\text{Yb}(\text{OTf})_2\text{-SO}_3\text{Na-MCMSS}$ catalyst.

Encouraged by these results, we examined the scope of the $\text{Yb}(\text{OTf})_2\text{-SO}_3\text{Na&Ph-MCSS}$ catalyzed Mukaiyama–Aldol coupling on a series of substrates. Similarly, 4-substituted benzaldehyde derivatives possessing either an electron-accepting group ($\text{NO}_2\text{-}$) or electron-donating group ($\text{CH}_3\text{O-}$) also led to high yields of the coupling products. Notably, 2-naphthaldehyde (with a large molecular size) could also be converted to product with an excellent yield of around 90%. Next, we investigated the conversion of aliphatic aldehydes with trimethyl-(1-phenylprop-1-enyloxy)silane, especially for water-soluble aldehydes, such as formaldehyde. As shown in Table 2, good yields were observed for all the aliphatic aldehydes. In the same way, the $\text{Yb}(\text{OTf})_2\text{-SO}_3\text{Na&Ph-MCSS}$ catalyst exhibited a higher catalytic activity and selectivity than those of the

Table 2 Catalytic performances of the different Yb catalysts in the water-medium Mukaiyama–Aldol reaction^a

				
Catalyst	R ₁	Conversion (%)	Selectivity (%)	Yield (%)
$\text{Yb}(\text{OTf})_2\text{-SO}_3\text{Na&Ph-MCMSS}$		92.5	99	92.4
$\text{Yb}(\text{OTf})_2\text{-SO}_3\text{Na-MCMSS}$		53.6	99	53.5
$\text{Yb}(\text{OTf})_2\text{-SO}_3\text{Na&Ph-MCSS}$		64.3	99	64.2
$\text{Yb}(\text{OTf})_2\text{-SO}_3\text{Na&Ph-MCMSS}$		95.5	99	95.4
$\text{Yb}(\text{OTf})_2\text{-SO}_3\text{Na-MCMSS}$		62.3	99	62.2
$\text{Yb}(\text{OTf})_2\text{-SO}_3\text{Na&Ph-MCSS}$		68.6	99	68.5
$\text{Yb}(\text{OTf})_2\text{-SO}_3\text{Na&Ph-MCMSS}$		90.0	99	89.9
$\text{Yb}(\text{OTf})_2\text{-SO}_3\text{Na-MCMSS}$		47.8	99	47.7
$\text{Yb}(\text{OTf})_2\text{-SO}_3\text{Na&Ph-MCSS}$		62.1	99	62.0
$\text{Yb}(\text{OTf})_2\text{-SO}_3\text{Na&Ph-MCMSS}$	C_5H_{11} ^b	95.2	99	95.1
$\text{Yb}(\text{OTf})_2\text{-SO}_3\text{Na-MCMSS}$	C_5H_{11} ^b	59.2	99	59.1
$\text{Yb}(\text{OTf})_2\text{-SO}_3\text{Na&Ph-MCSS}$	C_5H_{11} ^b	71.0	99	70.9
$\text{Yb}(\text{OTf})_2\text{-SO}_3\text{Na&Ph-MCMSS}$	H^b	92.1	84 ^c	77.3
$\text{Yb}(\text{OTf})_2\text{-SO}_3\text{Na-MCMSS}$	H^b	75.9	56	42.5
$\text{Yb}(\text{OTf})_2\text{-SO}_3\text{Na&Ph-MCSS}$	H^b	83.5	68	56.8

^a Reaction conditions: 0.50 mmol benzaldehyde, 1.0 mmol silane, 0.050 mmol Yb, 3.0 ml water, 20 °C, 16 h. ^b 10 mmol HCHO in 37% aqueous solution, 1.0 mmol silane. ^c The selectivity was determined based on its ratio to the byproduct propiophenone from the hydrolysis of silane.

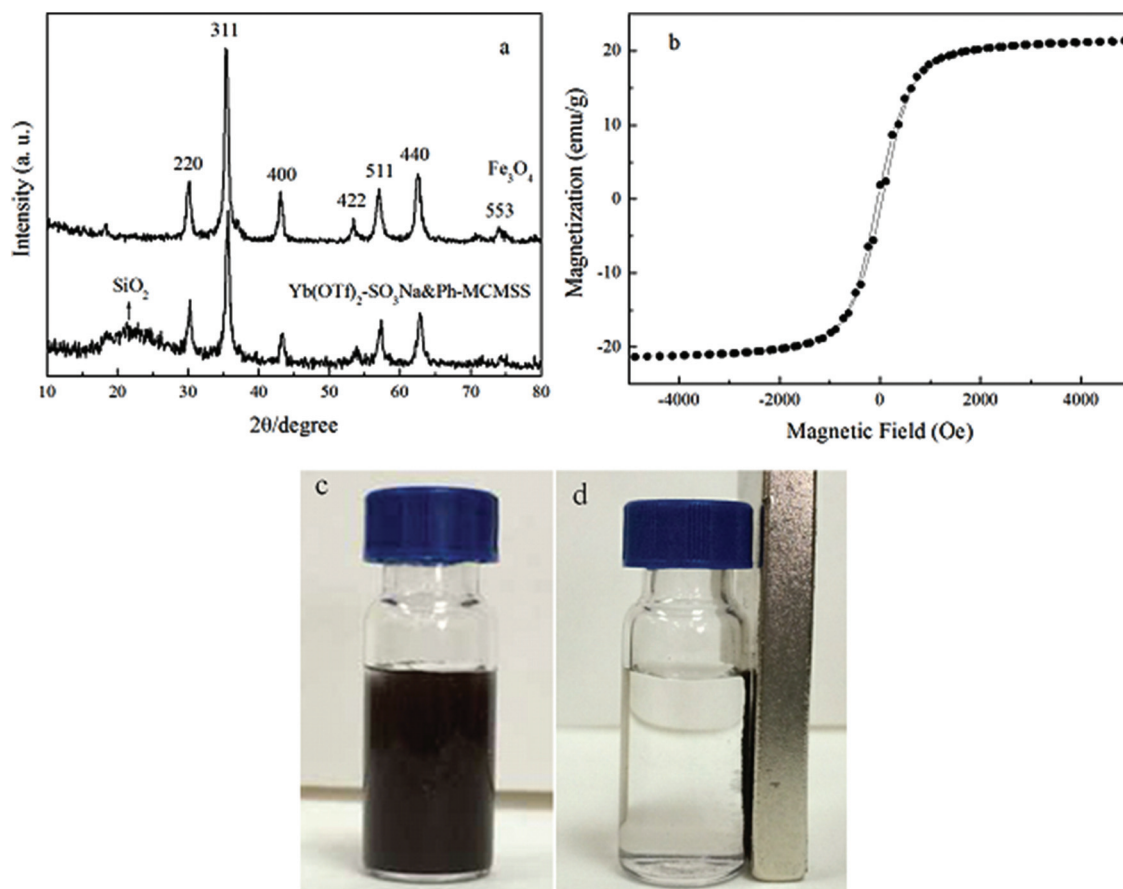


Fig. 9 (a) Wide-angle XRD patterns of the Fe_3O_4 and $\text{Yb}(\text{OTf})_2\text{-SO}_3\text{Na}\&\text{Ph-MCMSS}$ samples, (b) magnetization curve of the $\text{Yb}(\text{OTf})_2\text{-SO}_3\text{Na}\&\text{Ph-MCMSS}$ catalyst determined at room temperature, (c) the reaction mixture containing the $\text{Yb}(\text{OTf})_2\text{-SO}_3\text{Na}\&\text{Ph-MCMSS}$ catalyst, and (d) the reaction mixture containing the $\text{Yb}(\text{OTf})_2\text{-SO}_3\text{Na}\&\text{Ph-MCMSS}$ catalyst with the application of a magnet.

$\text{Yb}(\text{OTf})_2\text{-SO}_3\text{Na-MCMSS}$ and $\text{Yb}(\text{OTf})_2\text{-SO}_3\text{Na}\&\text{Ph-MCSS}$ catalysts for all the reactants, demonstrating its universal advantage in the water-medium Mukaiyama–Aldol reaction.

To determine whether the heterogeneous or the dissolved homogeneous $\text{Yb}(\text{III})$ compound was the real acid active species, the procedure proposed by Sheldon group was carried out.²⁵ After reacting for 8 h the conversion exceeded 50% in the Mukaiyama–Aldol reaction between benzaldehyde and trimethyl-(1-phenylprop-1-enyloxy)silane, the mixture was separated by an external magnet to remove the solid catalyst and then the mother liquor was allowed to react for another 10 h under the same reaction conditions. No significant change in the benzaldehyde conversion was observed, suggesting that the catalytic reactivity by the leaching $\text{Yb}(\text{III})$ catalyst could be approximately excluded in the present reaction. Moreover, the liquid phase of the reaction mixture was collected after each reaction. ICP-AES analysis confirmed a very low amount of Yb (less than 2.0 ppm) in the reaction mixture. Even if a long time reaction (36 h) was carried out or a large amount of the catalyst (0.50 g) was added, a low Yb leaching amount (less than 3.5 ppm) was detected after reaction in both cases. Therefore, the present catalysis was indeed heterogeneous in nature

rather than the result of any dissolved acid species leached from the $\text{Yb}(\text{OTf})_2\text{-SO}_3\text{Na}\&\text{Ph-MCSS}$ catalyst.

An attractive advantage of the $\text{Yb}(\text{OTf})_2\text{-SO}_3\text{Na}\&\text{Ph-MCSS}$ catalyst is its easy separation using an external magnet, which drastically reduces the operating time and costs arising from the separation of products from a reaction mixture. The reusability of the magnetic mesoporous catalysts relies on their magnetic-response property, since the external coating on the Fe_3O_4 surface usually decreased their magnetic responsivity.²⁶ The wide-angle XRD pattern exhibited well resolved diffraction peaks for the $\text{Yb}(\text{OTf})_2\text{-SO}_3\text{Na}\&\text{Ph-MCMSS}$ catalyst (Fig. 9a). All the peaks can be exactly indexed to the diffractions of the Fe_3O_4 crystal in the cubic spinel structure, suggesting that the coating process and surface modification have no effect on the crystal-line properties of magnetite. We furthermore analyzed its magnetic behavior using a magnetometer at 300 K (Fig. 9b). The results indicated that the $\text{Yb}(\text{OTf})_2\text{-SO}_3\text{Na}\&\text{Ph-MCMSS}$ catalyst had a magnetization saturation value of 21.3 emu g^{-1} , demonstrating its superparamagnetic behavior.²⁷ Thus, it could simply be recovered in a short time (<10 s) by fixing a magnet near to the reaction vessel (Fig. 9c and d). Fig. 10 shows the recyclability of the $\text{Yb}(\text{OTf})_2\text{-SO}_3\text{Na}\&\text{Ph-MCMSS}$ catalyst during

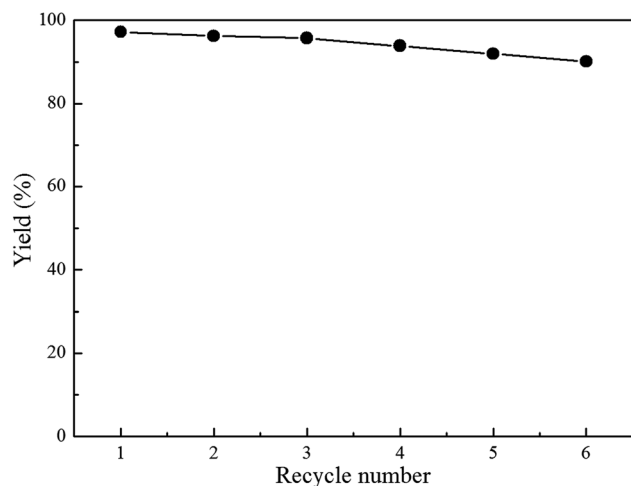


Fig. 10 The recycling tests of the $\text{Yb}(\text{OTf})_2\text{-SO}_3\text{Na\&Ph-MCMSS}$ catalyst in the water-medium Mukaiyama–Aldol reaction. Reaction conditions are given in Table 1.

the water-medium Mukaiyama–Aldol reaction between benzaldehyde and trimethyl-(1-phenylprop-1-enyloxy)silane. No remarkable decrease could be observed in the catalytic activity after being used repetitively six times, revealing its superiority over the corresponding $\text{Yb}(\text{OTf})_3$ homogeneous catalyst for reducing the cost and environmental pollution from homogeneous acid and organic solvents. The ICP analysis confirmed that only about 4.8% of the Yb species leached off after six cycles in the recycled $\text{Yb}(\text{OTf})_2\text{-SO}_3\text{Na\&Ph-MCMSS}$ catalyst, demonstrating that the existence of the mesoporous structure could effectively restrict the leaching of active sites.²⁸ In addition, the N_2 sorption isotherm and low-angle XRD pattern (Fig. S5†) confirmed that the ordered 2-D mesostructure and high surface area were also well preserved. Moreover, the TEM image (Fig. S6†) of the recycled $\text{Yb}(\text{OTf})_2\text{-SO}_3\text{Na\&Ph-MCMSS}$ catalyst after six repetitions indicated that it could retain the spherical morphology and mesoporous structure and only partial particle aggregation existed, suggesting the relatively high structure stability in water-medium organic synthesis.

4. Conclusion

In summary, we have developed a novel approach to prepare a highly active and water-compatible magnetic mesoporous Lewis acid catalyst ($\text{Yb}(\text{OTf})_2\text{-SO}_3\text{Na\&Ph-MCMSS}$) by introducing $\text{Yb}(\text{OTf})_3$ into the mesoporous channels of a SO_3Na - and Ph-functionalized magnetic core–silica shell support. Notably, it displayed a remarkable enhancement in the catalytic activity for the water-medium Mukaiyama–Aldol reaction compared to the homogeneous $\text{Yb}(\text{OTf})_3$ catalyst. In comparison to the $\text{Yb}(\text{OTf})_2\text{-SO}_3\text{Na-MCMSS}$ catalyst without phenyl groups inside the mesoporous channels, $\text{Yb}(\text{OTf})_2\text{-SO}_3\text{Na\&Ph-MCSS}$ catalyst without a mesoporous structure, $\text{Yb}(\text{OTf})_2\text{-SO}_3\text{Na-MCM-41}$ mesoporous catalyst with an irregular morphology and nonporous $\text{Yb}(\text{OTf})_2\text{-SO}_3\text{Na-Amberlyst-15}$ ion-exchange resin catalyst, it also

exhibited a higher catalytic reactivity and selectivity. Control experiments and systematic characterizations confirmed that its unique mesoporous confinement effect and surface hydrophobicity could enrich the reactants and simultaneously reduce the diffusion transfer limitation in water, resulting in the enhanced catalytic efficiency. Moreover, it could be easily recycled using an external magnet and reused at least six times without loss of catalytic activity. This work provides a novel synthetic approach towards the preparation of highly efficient and easily recyclable heterogeneous catalysts for more environmentally friendly chemical transformations.

Acknowledgements

This work was supported by the Natural Science Foundation of China (21107071 and 51273112), PCSIRT (IRT1269) and the Shanghai Government (13QA1402800 and 12CG52).

Notes and references

- 1 J. A. Melero, R. van Grieken and G. Morales, *Chem. Rev.*, 2006, **106**, 3790–3812.
- 2 T. M. Jyothi, M. L. Kaliya and M. V. Landau, *Angew. Chem., Int. Ed.*, 2001, **40**, 2881–2884.
- 3 A. Corma and H. García, *Chem. Rev.*, 2003, **103**, 4307–4365.
- 4 R. N. Butler and A. G. Coyne, *Chem. Rev.*, 2010, **110**, 6302–6337.
- 5 K. Inumaru, T. Ishiharam, Y. Kamiya, T. Okuhara and S. Yamanaka, *Angew. Chem., Int. Ed.*, 2007, **46**, 7625–7628.
- 6 F. D. Clippel, M. Dusselier, S. V. D. Vyver, L. Peng, P. Jacobs and B. F. Sels, *Green Chem.*, 2013, **15**, 1398–1430.
- 7 J. P. Ge, T. Huynh, Y. X. Hu and Y. D. Yin, *Nano Lett.*, 2008, **8**, 931–934.
- 8 (a) V. Polshettiwar, R. Luque, A. Fihri, H. B. Zhu, M. Bouhrara and J. M. Basset, *Chem. Rev.*, 2011, **111**, 3036–3075; (b) S. Shylesh, V. Schünemann and W. R. Thiel, *Angew. Chem., Int. Ed.*, 2010, **49**, 3428–3459; (c) M. B. Gawande, P. S. Brance and R. S. Varma, *Chem. Soc. Rev.*, 2013, **42**, 3371–3393.
- 9 M. Feyen, C. Weidenthaler, F. Schüth and A. H. Lu, *Chem. Mater.*, 2010, **22**, 2955–2961.
- 10 F. C. Zheng, Q. W. Chen, L. Hu, N. Yan and X. K. Kong, *Dalton Trans.*, 2014, **43**, 1220–1227.
- 11 (a) J. Liu, S. Z. Qiao, Q. H. Hu and G. Q. Lu, *Small*, 2011, **7**, 425–443; (b) J. P. Ge, Q. Zhang, T. R. Zhang and Y. D. Yin, *Angew. Chem., Int. Ed.*, 2008, **47**, 8924–8928; (c) A. H. Lu, W. Schmidt, N. Matoussevitch, H. Boennemann, B. Spliethoff, B. Tesche, E. Bill, W. Kiefer and F. Schüeth, *Angew. Chem., Int. Ed.*, 2004, **43**, 4303–4306; (d) D. Damodara, R. Arundhatiab and P. R. Likhar, *Catal. Sci. Technol.*, 2013, **3**, 797–802; (e) H. Q. Yang, Y. W. Wang, Y. Qin, Y. Z. Chong, Q. Z. Yang, G. Li, L. Zhang and W. Li, *Green Chem.*, 2011, **13**, 1352–1361; (f) R. B. Nasir Baig and R. S. Varma, *Green Chem.*, 2013, **15**, 398–417; (g) Z. M. Cui, Z. Chen, C. Y. Cao, L. Jiang and W. G. Song, *Chem.*

- Commun.*, 2013, **49**, 2332–2334; (h) J. H. Yang, D. F. Wang, W. D. Liu, X. Zhang, F. L. Bian and W. Yu, *Green Chem.*, 2013, **15**, 3429–3437; (i) H. R. Shaterian and M. Aghakhanizadeh, *Catal. Sci. Technol.*, 2013, **3**, 425–428.
- 12 (a) Y. H. Deng, Y. Cai, Z. K. Sun, J. Liu, C. Liu, J. Wei, W. Li, C. Liu, Y. Wang and D. Y. Zhao, *J. Am. Chem. Soc.*, 2010, **132**, 8466–8473; (b) S. Okada, S. Ikurumi, T. Kamegawa, K. Mori and H. Yamashita, *J. Phys. Chem. C*, 2012, **116**, 14360–14367; (c) Y. Chi, Q. Yuan, Y. J. Li, L. Zhao, N. Li, X. T. Li and W. F. Yan, *J. Hazard. Mater.*, 2013, **262**, 404–411; (d) P. Li, Y. Yu, H. Liu, C. Y. Cao and W. G. Song, *Nano-scale*, 2014, **6**, 442–448.
 - 13 S. Shylesh, L. Wang, S. Demeshko and W. R. Thiel, *ChemCatChem*, 2010, **2**, 1543–1547.
 - 14 C. S. Gill, B. A. Price and C. W. Jones, *J. Catal.*, 2007, **251**, 145–152.
 - 15 Q. H. Yang, M. P. Kapoor and S. Inagaki, *J. Am. Chem. Soc.*, 2002, **124**, 9694–9695.
 - 16 R. Kumar, J. P. Sharma and S. S. Sekhon, *Eur. Polym. J.*, 2005, **41**, 2718–2725.
 - 17 S. Suga, S. Ogawa, H. Namatame, M. Taniguchi, A. Kakizaki, T. Ishii, A. Fujimori, S. J. Oh, T. Miyahara, A. Ochiai, T. Suzuki and T. Kasuya, *J. Phys. Soc. Jpn.*, 1989, **58**, 4534–4543.
 - 18 D. Y. Zhao, J. L. Feng, Q. S. Huo, N. Melosh, G. H. Fredrickson, B. F. Chmelka and G. D. Stucky, *Science*, 1998, **279**, 548–552.
 - 19 K. Nakajima, I. Tomita, M. Hara, S. Hayashi, K. Domen and J. N. Kondo, *Adv. Mater.*, 2005, **17**, 1839–1842.
 - 20 S. B. Jennifer Kan, K. K. H. Ng and I. Paterson, *Angew. Chem., Int. Ed.*, 2013, **52**, 9097–9108.
 - 21 R. Siegel, E. Domingues, R. De Sousa, F. Jérôme, C. M. Morais, N. Bion, P. Ferreira and L. Mafra, *J. Mater. Chem.*, 2012, **22**, 7412–7419.
 - 22 F. Zhang, J. Yin, W. Chai and H. X. Li, *ChemSusChem*, 2010, **3**, 724–727.
 - 23 W. H. He, F. Zhang and H. X. Li, *Chem. Sci.*, 2011, **2**, 961–966.
 - 24 M. Sanlés-Sobrido, M. Pérez-Lorenzo, B. Rodríguez-González, V. Salgueiriño and M. A. Correa-Duarte, *Angew. Chem., Int. Ed.*, 2012, **51**, 3877–3882.
 - 25 R. A. Sheldon, M. I. Wallau, W. C. E. Arends and U. Schuchardt, *Acc. Chem. Res.*, 1998, **31**, 485–493.
 - 26 M. Shokouhimehr, Y. Piao, J. Kim, Y. Jang and T. Hyeon, *Angew. Chem., Int. Ed.*, 2007, **46**, 7039–7043.
 - 27 M. J. Jin and D. H. Lee, *Angew. Chem., Int. Ed.*, 2010, **49**, 1119–1022.
 - 28 P. Sreekanth, S. Kim, T. Hyeon and B. Kim, *Adv. Synth. Catal.*, 2003, **345**, 936–938.